Measurements of Bubble Size Distributions with an Optical Technique Based on Depth from Focus

Peter Geißler[1] *and Bernd Jähne*[1,2]

[1]Interdisciplinary Center for Scientific Computing, University of Heidelberg
Im Neuenheimer Feld 368, 69120 Heidelberg, Germany
email: pgeiss@giotto.iwr.uni-heidelberg.de
[2]Scripps Institution of Oceanography, Physical Oceanography Res. Div.
La Jolla, CA 92093-0230, USA
email: bjaehne@ucsd.edu

Abstract

An optical sensor for bubble size measurements is presented. It is based on the combination of light blocking visualization and depth from focus techniques and allows for the measurement of single bubbles. The degree of blur in the images of single bubbles is used to compute the distance from focal plane and thus to determine a virtual measuring volume that is increasing with bubble size. The image sequences are evaluated using digital image processing to calculate bubble size distributions. Experiments performed in the linear wind/wave facility of Delft Hydraulics are presented. For different wind speed conditions and depths bubble spectra in fresh water have been measured.

1 Introduction

Air bubbles are produced in the upper regions of the ocean by air entrainment due to breaking waves. These bubbles play an important role in various small-scale air-sea interaction processes, especially for the exchange of climate relevant trace gases such as O_2 and CO_2 at high wind conditions. By offering an additional route for gas exchange, the presence of bubbles leads to a significantly enhanced transfer velocity [*Liss and Merlivat*, 1986]. This has recently confirmed in field experiments [*Farmer*, 1993], as well as in several laboratory studies in whitecap simulation tanks by *Monahan* [1990] and *Asher* [1991]. The influence of bubbles depends greatly on parameters as buoyancy (and thus lifetime) and amount of gas carried by the bubble, which are given by the size of the bubble. Small bubbles tend to completely disappear by dissolution in the water. Large bubbles exchange gas through their surface towards equilibrium. The importance of large bubbles to gas exchange has first been pointed out by *Jähne*, [1984]. Recently, *Keeling*, [1993] introduced a detailed model for bubble mediated gas exchange. It indicates that bubbles with radii greater than 500 μm contribute significantly

B. Jähne and E. Monahan (eds.), Air-Water Gas Transfer, © *1995 by AEON Verlag*

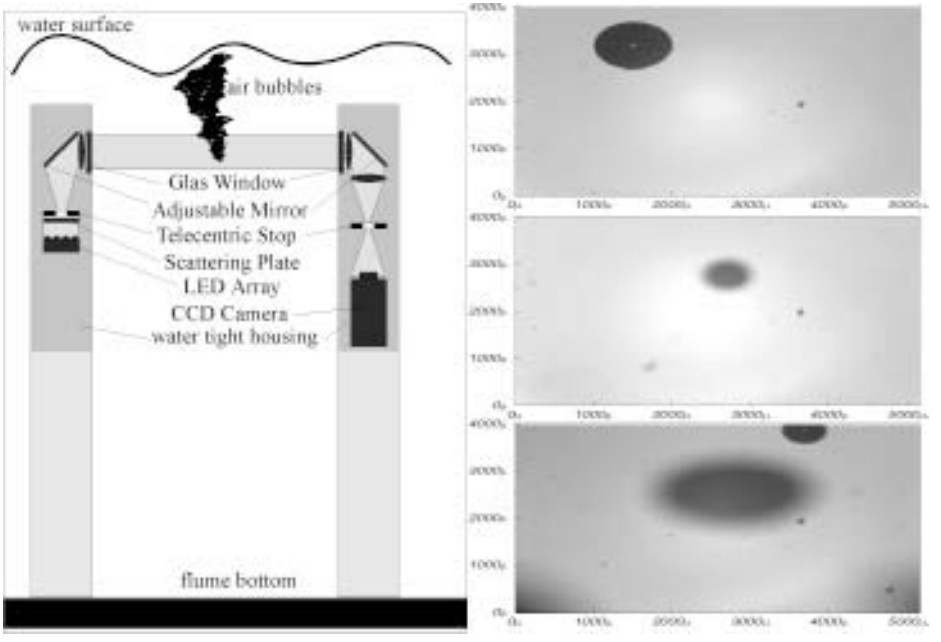

Figure 1: left: Sketch drawing of the optical bubble measuring device used during the second campaign in the Delft facility. right: Three images taken with the direct light illumination technique. Both well focused and out of focus bubbles can be seen.

to bubble induced gas transfer and oceanic supersaturation of more soluble gases. Furthermore, the transfer velocity becomes dependent on both molecular diffusivity and solubility. Uncertainties in the model arise from the lack of information about bubble distributions in the open sea. Therefore it is necessary to measure both bubble spectra and depth distributions at various wind speed conditions, especially for larger bubble sizes.

We have developed an optical device to measure the sizes of single bubbles in a diameter range of 50 μm to 1000 μm. It was used during a measuring campaign in the large wind wave facility of Delft Hydraulics in the fall of 1991 and 1994. The main feature of the device is that the measuring volume can be defined without the help of mechanical delimiters. Furthermore, it increases linearly with bubble size. Due to the typical decrease of the bubble density with the radius ($\sim r^{-2}$ - r^{-4}), this significantly enhances the statistics for large bubbles. Recently, *de Leeuw* [1994] used a similar system for field measurements in the North Sea. It uses a similar illumination technique, but the measuring volume is defined by mechanical delimiters and independent of bubble size.

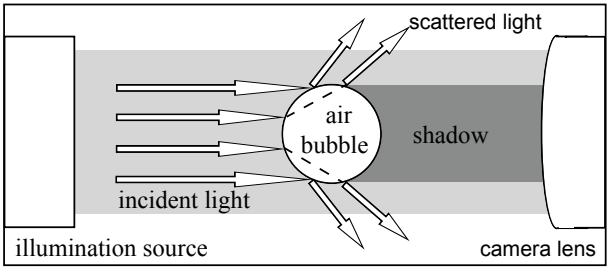

Figure 2: Visualization principle: bubbles scatter light so that it does not reach the lens (not drawn to the scales).

2 The Measuring System

The device consists of two water tight housings, mounted to the bottom of the flume in a distance of 40 cm (Figure 1). The vertical position of the device can be changed, thus allowing the measurement of bubble size distribution at various depths to the mean water surface. One of the housings contains the illumination system, while the optical receiver is located in the other one. The sample volume is located in between the both towers. The air bubbles are imaged using a CCD camera looking directly into the light source. Light hitting an air bubble in the measuring volume is scattered so that it does not reach the camera lens. Therefore, a dark image of the bubble is obtained on the image plane, allowing the determination of the shape of each individual bubble (Figures 2 and 1).

The illumination consists of an array of 7 LED's. Synchronized with the image acquisition, they were pulsed with a duration of 20 μs. In addition, the camera is shuttered to an acquisition time of 1/2000 s to completely suppress scattered light from the environment. The short illumination time avoids any motion blur in the images of fast moving bubbles. With a single pixel imaging an area of 10.1 μm $\times$ 16.7 μm, bubble velocities up to 0.5 m/s (x-direction) and 0.8 m/s (y-direction) cause motion blur less than one pixel. Images sequences of 5000 to 8000 images were taken for each measuring condition. They were stored on laser video discs for later processing.

Due to the fact that the depth of field is small compared to the distance between the two towers, most bubbles are not in focus and thus imaged blurred. The measurement of the amount of the blur is used to calculate their position along the optical axis. From this the measuring volume can be determined. A principal problem of this approach is that it is not possible to distinguish whether a bubble is located in front or behind the focal plane. The calculation of the true size of a bubble from its blurred size and the amount of blur may therefore result in an ambiguity of the radius measurement. To overcome this problem, we used with the device of the 1994 campaign a telecentric path of rays both on the illumination side as well as

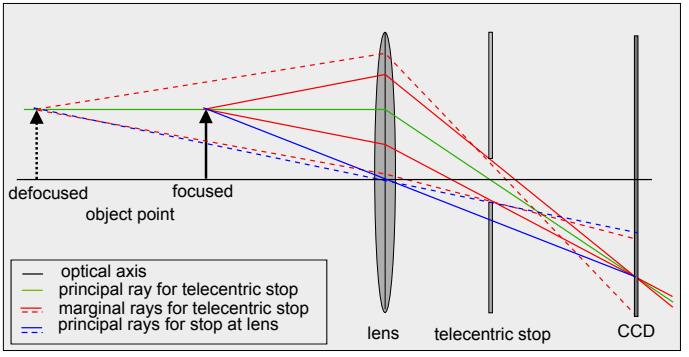

Figure 3: Principle of the telecentric optics: the displacement of an object point along the optical axis does not cause changes in the size of the image.

on the camera side. With this setup, the aperture stop is located at the rear focal point of the respective optics. The effect is that all principal rays in object space are parallel to the optical axis. Only narrow and axis-parallel ray bundles contribute to image formation. Then, the size of blurred bubbles becomes independent from the grade of the blur or the location along the optical axis (Figure 3). The size of a blurred bubble is hereby defined at the gray values that are the half of the maximum gray value. Furthermore, the grade of blurring becomes independent from whether the position is in front or behind the focal plane. Because of the symmetry introduced by the telecentric path of rays, the position ambivalence can be completely disregarded in the measurements.

3 Determination of Bubble Size Distributions

3.1 Principle

Bubble size distributions can be calculated from the image sequences if both the size of each individual bubble as well as the measuring volume is known. The volume can be calculated if the 3D-positions of every bubble are known. The calculation of the position perpendicular to the optical axis is trivial: it is directly given by the gray value center of the bubble in the image. The position along the axis can be determined from a single two-dimensional image using a *depth-from-focus* technique [*Jähne and Geißler*, 1994]: because the depth of field of the optical system is small compared to the distance between the focal plane and the lens, only the images of bubbles closed to the focal plane appear sharp. The blur in the image increases with the distance of the bubble from the focal plane. Therefore, the measurement of the blur allows us to determine the position along the optical axis. Because a large bubble at the same distance from the focal plane appears less blurred

than a smaller one, a "minimum sharpness" criterion yields a measuring volume with is roughly proportional to the bubble diameter. Furthermore, the "virtual volume boundaries" avoid all the disadvantages of flow distortions caused by mechanical volume delimiters close to the measuring volume.

3.2 Model of Image Formation

An air bubble can be modelled by its light absorbing coefficient $\tau(\vec{x})$ in the object plane. A circular bubble at the position $\vec{X}_0$ and with the radius r is then described as a circular box function $\tau(\vec{X}) = \Pi\left(|\vec{X} - \vec{X}_0|/2r\right)$ where $\Pi(x)$ is the unit step function. The capital letters indicate object plane coordinates. The Z axis of the system coincides with the optical axis of the system. The image of the bubble is given by the convolution of the well focused image with the *point spread function* $PSF(\vec{x})$ of the optical system:

$$I(\vec{x}) = \left(1 - \Pi\left(\frac{|\vec{x} - \vec{x}_0|}{2r}\right)\right) * PSF(\vec{x}). \tag{1}$$

In this equation, the object coordinates have been replaced by the image coordinates. With the telecentric path of rays, the geometrical magnification is independent of z and is taken here as 1 for convenience. With increasing z, the point spread function does not change its shape but only its extension. Therefore, the normalized PSF is given by

$$PSF_z(\vec{x}) = kB\left(\frac{\vec{x}}{V_p(z)}\right) \tag{2}$$

with the normalization factor $k^{-1} = \int d\vec{x} B(\vec{x})$.

At the focal plane ($z = 0$), V_p is 0 resulting in delta peak for the PSF. The resulting brightness distribution on the CCD sensor plane is then

$$I(\vec{x}) = v(\vec{x})\left[1 - \tau\left(\vec{x}\right) * PSF_z(\vec{x})\right] \tag{3}$$

with $v(\vec{x})$ being the vignetting function.

3.3 Gray-Scale Normalization

First, the quantity of interest $\tau\left(\vec{x}\right) * PSF_z(\vec{x})$ has to be extracted from the acquired images. This is done by applying a linear illumination model assuming that the image shows a background level $b(\vec{x})$ and that the measured gray values $g(\vec{x})$ are further proportional to the irradiance $I(\vec{x})$. Then

$$g(\vec{x}) = a(\vec{x})I(\vec{x}) + b(\vec{x}). \tag{4}$$

The unknown quantities $b(\vec{x})$ and $a(\vec{x})$ are obtained by taking a background image $g_b(\vec{x})$ with illumination switched off ($I(\vec{x}) = 0$) and a zero image $g_z(\vec{x})$ in which no bubbles are present ($I(\vec{x}) = I_0(\vec{x})$).

Then, the linear inhomogeneous point operation

$$n(\vec{x}) = \frac{g_z(\vec{x}) - g(\vec{x})}{g_z(\vec{x}) - g_b(\vec{x})} = \tau\,(\vec{x}) * PSF_z(\vec{x}) \tag{5}$$

results in a normalized gray value $n(\vec{x})$ in the range of 0 to 1. It is important to note that this procedure removes any type of inhomogeneities caused by uneven illumination or small dust particles on the CCD chip or the lenses.

3.4 Measurement of Size and Distance from Focal Plane

As mentioned above, the size of a bubble can be calculated from its blurred image if the boundary is defined to be at the gray values which are $1/2$ of the maximum gray value. The radius is calculated from the segmented area A as the area equivalent radius $\sqrt{A/\Pi}$.

To determine the distance from the focal plane, it is necessary to measure the amount of blurring in the image. A good integral measure of the blur of a bubble is the mean gray value g_m on the $1/2$-area, which is one for a well focused bubble and decreases with increasing distance from the focal plane. All bubbles with the same ratio between the radius r and the size V_p of the point spread function have the same mean gray value g_m, because their images differ only in size and are of the same shape. Thus,

$$\frac{V_p(z)}{r} = const \Leftrightarrow g_m = const. \tag{6}$$

Denoting the constant in the above equation by $\gamma(g_m)$, g_m is given by

$$g_m(z, r) = \gamma^{-1}\left(\frac{V_p(z)}{r}\right) \tag{7}$$

Because due to the telecentric path of rays, $V_p(z)$ is a symmetric and linear function of z. Therefore, g_m depends only on the normalized distance z/r:

$$g_m(z, r) = \gamma^{-1}\left(\frac{a|z|}{r}\right) = g_m\left(\frac{|z|}{r}\right) \tag{8}$$

Thus, together with the direct radius measurement g_m allows the measurement of the distance $|z|$ from the focal plane.

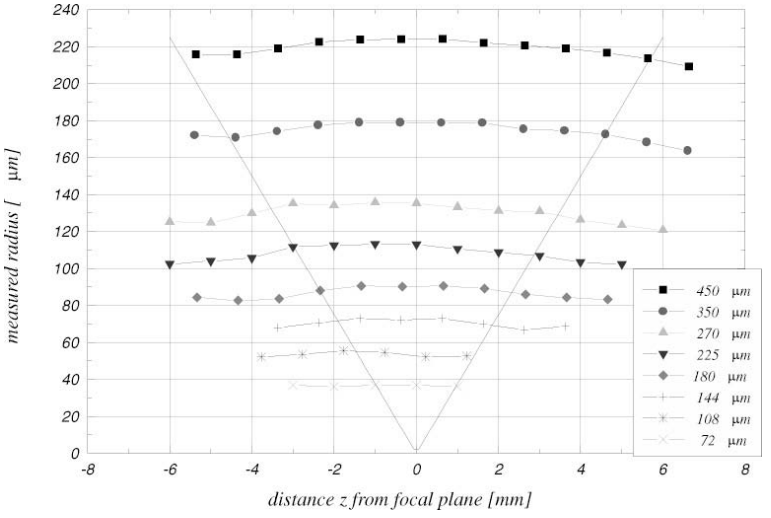

Figure 4: Independence of the size of blurred bubbles with the distance from the focal plane. The thin lines indicate the size of the virtual measuring volume.

4 Calibration

Calculating bubble size distributions from the image sequences with the depth from focus approach requires that the instrument is calibrated with a focus series of calibration targets of known size. Patterson reticles were used as calibration targets.

This standard target for microscopic calibration consists of a series of black circles in a diameter range from 18 μm up to 450 μm on a glass plate. Because Patterson globes are not absolutely accurate, the true size of each circle has to be measured independently, e.g. using a calibrated microscope. A black circle is a very good approximation of the focused image of a bubble, since with the optical setup used in the experiments more than 99.6% of the incident light is scattered away from the receiver. Nevertheless, the bright dot which appears in the center of well focused bubbles can be easily removed by applying a median filter to the normalized image before computing the mean gray value. To perform the calibration, an optical bench is mounted on top of the device. The calibration target is then fixed to the bench with a precision positioning table. Depth series centered to the focal plane are taken with a step size of 1 mm. Figure 4 shows the radii measured from different circles of the patterson target. Within the measuring volume, the difference between the measured and the true radius in in the order of 10 to 15 μm, which is about the size of one pixel. The variation of the mean gray value with increasing depth is shown in Figure 5. A linear model $g(z,r) = g_0 - \alpha(r)|z|$ fits well to the data. Because a small axis offset and slight tilt of the target can often not be avoided, the axis offset for each

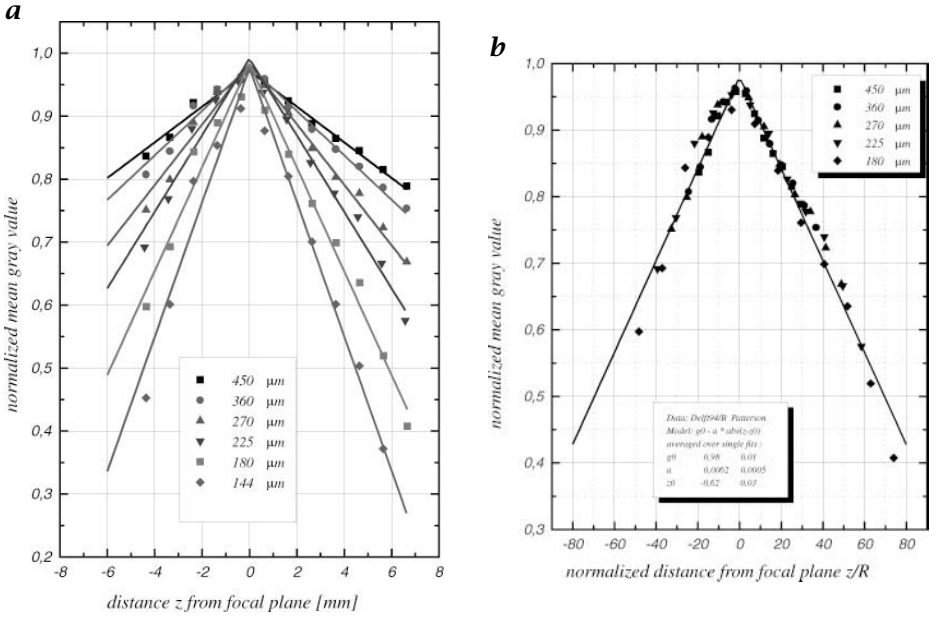

Figure 5: ***a*** *mean gray value calculated for different patterson globes;* ***b*** *mean gray value versus normalized distance z/R. This validates the fact that g_m only depends on z/R.*

circle is corrected by finding the center of symmetry in its depth series.

5 Measuring Volume

The decrease of the mean gray value with increasing distance from the focal plane can now be used to define the measuring volume by a lower limit for g_m. Only bubbles with mean gray values above this limit are taken into account for the calculation of the size distribution. Thus the linear dependence of g_m on the normalized distance

$$g(z,r) = g_0 - \alpha(r)|z| = g_0 - \alpha_0 \frac{|z|}{r} \tag{9}$$

gives the volume boundary:

$$z_{max} = \frac{1}{\alpha(r)}(1 - g_{min}) = \frac{r}{\alpha_0}(1 - g_{min}). \tag{10}$$

The measuring volume is then given by

$$V(r) = 2z_{max}(r)A_0 \tag{11}$$

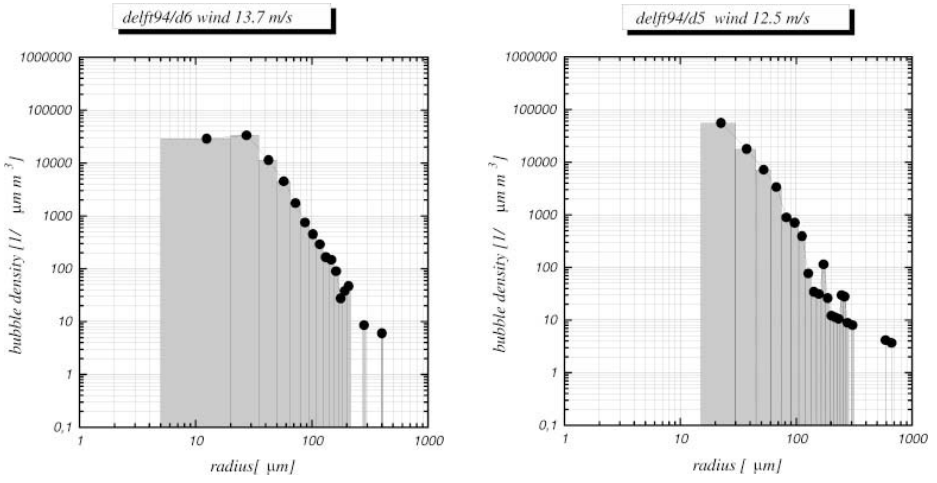

Figure 6: Size distributions of bubbles measured 5.5 cm below the mean water surface at wind speeds of 13.7 m/s and 12.5 m/s in the wind/wave flume of Delft Hydraulics, The Netherlands. The gray bars indicate the width of the histogram bins.

with A_0 being the area imaged by the CCD at the focal plane.

Due to the fact that bubbles touching the border of the image cannot be processed at the moment, the measuring volume increases approximately linear with the radius for smaller bubbles (up to a radius of approx. 300 μm) only.

6 Results

The bubble measuring device has been used in the large wind wave facility of Delft Hydraulics. Bubble spectra were measured under wind speed conditions from 7 m/s up to 14 m/s and depths from 3 cm to 30 cm. For all measuring conditions, fresh water was used. The flume is described in detail in *van Vliet et al.* [1995].

Two sample spectra are shown in Figure 6. These were measured at wind speeds of 13.5 m/s and 12.5 m/s in a mean water depth of 5.5 cm. Both show a steep decrease of the bubble density towards larger radii approximately with $r^{-3.3}$.

The bubble size distributions were calculated from the number $N(r, dr)$ of bubbles found in the radius interval $[r, r + dr]$ by

$$\psi(r, dr) = \frac{N(r, dr)}{N_I dr V(r)} \tag{12}$$

where N_I is the total number of images. A bin size of 15 μm has been used to calculate the size distributions. In Figure 7 size distributions are shown

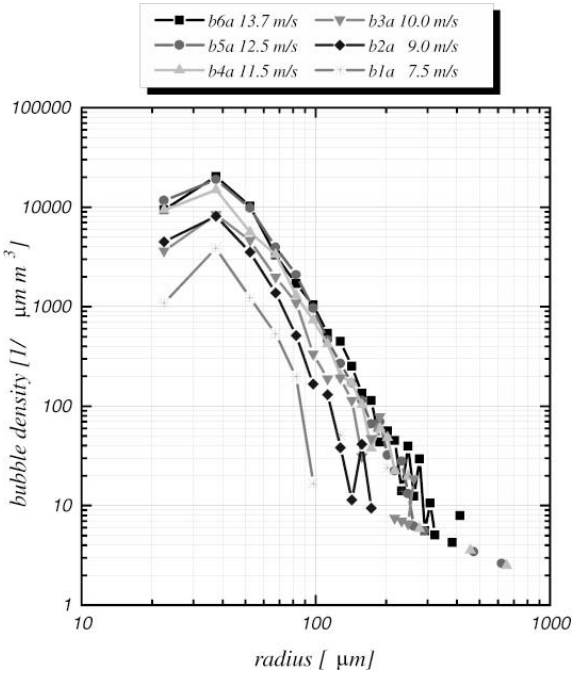

Figure 7: Size distributions of bubbles measured at different wind speeds 17.5 cm below the mean water surface in the wind/wave flume of Delft Hydraulics, The Netherlands.

over a wider wind speed range. These spectra have been measured at the same location within the flume, but at a depth of 17.5 cm.

All spectra show a cutoff at small bubble sizes. Because all cutoff radii are in the range of 20 – 40 μm and thus belonging to a pixel area of less then 25 pixels, it is very likely that the cutoff is an artifact introduced by the fact that the segmentation is performed on a coarse grid. No subpixel accurate segmentation can be done at the moment. For bubble radii greater than 500 μm, the number of bubbles per bin is to small to allow for the computation of the size distribution. The comparison between bubble spectra measured at different depth to the mean water level implies that the total number of bubbles does not change with depth. In fact, this is not true because for the smaller depth the measuring volume comes up in wave trudges. Instead of the number of acquired images the number of in-water images has to be used in (12). A coarse estimate shows that then the total number of bubbles is different by about a factor of 30 – 40 %.

7 Conclusions

In this paper an optical sensor for bubble size measurements has been introduced. It has been showed that the combination of direct visualization of single bubbles and a depth from focus approach to define a non-mechanical delimited measuring volume allows the construction of a rugged bubble measuring device.

The use of a telecentric path of rays is a significant improvement compared to the device we used in the first measuring campagain. It allows for easier calibration and direct measurement of bubble radii. A not yet solved problem is the fixed measuring position that does not allow for measurements of bubble size distributions in a constant distance to the water surface, but averages over a depth range according to the wave height. This problem can be solved by either parallel measuring of the actual wave height or by mounting the device on a float which moves with the larger waves. Therefore it is intended to use the sensor on a drifting buoy to measure bubble spectra at sea.

Acknowledgements

Financial support of the European Community (Large Installation Program) that enabled us to perform measurements at the wind/wave flume of Delft Hydraulics, The Netherlands, is gratefully acknowledged.

References

Asher, W., E. Monahan, R. Wanningkof, and T. Bates, Correlation of Fractional Foam Coverage with Gas Transport Rates, *Air-Water Mass Transfer*, selected papers from the 2nd International Symposium on Gas Transfer at Water Surfaces, Minneapolis, S. Wilhelms and J. Gulliver, eds., pp. 536-548, ASCE, New York., 1990

Farmer, D. M., C. L. McNeil, and B. D. Johnson, Evidence for the importance of bubbles in increasing air-sea gas flux, *Nature*, 361, 620–623, 1993.

Jähne, B., T. Wais, and M. Barabas, A New Optical Bubble Measuring Device; A Simple Model for Bubble Contribution to Gas Exchange, *in: Gas Transfer at Water Surfaces*, W. Brutsaert and G. Jirka, eds, pp. 237-246, Reidel Publishing Company, 1984

Jähne, B., and P. Geißler, Depth from focus with one image, Proc_*Conference on Computer Vision and Pattern Recognition (CVPR'94)*, Seattle, 20.–23. June 1994, 713–717, 1994

Keeling, R., On the role of large bubbles in air-sea gas exchange and supersaturation in the ocean, *Journal of Marine Research*, *51*, 237–471, 1993.

Liss, P. S., and Merlivat, L. Air-Sea gas exchange rates : introduction and synthesis, *The Role of Air-Sea Exchange in Geochemical Cycling*, edited by P. Buat-Menard, pp. 113-127, Reidel Publishing Company, 1986

de Leeuw, G., and L. Cohen, Measurements of oceanic bubble size distributions, *Oceans 94, 13-16 Sept. 1994*

Monahan, E., and T. Torgersen, The Enhancement of Air-Sea Gas Exchange by Oceanic Whitecapping *Air-Water Mass Transfer*, selected papers from the 2nd International Symposium on Gas Transfer at Water Surfaces, Minneapolis, Minnesota, S. Wilhelms and J. Gulliver, eds, pp. 608-617, ASCE, New York., 1990

van Vliet, P., F. Hering, and B. Jähne, Delft Hydraulic's large wind/wave flume, *This volume*